The chloride channel cystic fibrosis transmembrane conductance regulator (CFTR) controls cellular quiescence by hyperpolarizing the cell membrane during diapause in the crustacean *Artemia*

Received for publication, September 19, 2018, and in revised form, February 10, 2019 Published, Papers in Press, February 14, 2019, DOI 10.1074/jbc.RA118.005900

An-Qi Li[‡], Zhan-Peng Sun[‡], Xu Liu[‡], Jin-Shu Yang[‡], Feng Jin[‡], Lin Zhu[‡], Wen-Huan Jia[‡], Stephanie De Vos[§], Gilbert Van Stappen[§], Peter Bossier[§], and Wei-Jun Yang[‡¶1]

From the [‡]College of Life Sciences, Zhejiang University, Hangzhou, Zhejiang 310058, China, the [§]Laboratory of Aquaculture and Artemia Reference Center, Department of Animal Production, Ghent University, B-9000 Ghent, Belgium, and the [¶]Laboratory for Marine Biology and Biotechnology, Qingdao National Laboratory for Marine Science and Technology, Qingdao 266000, China

Edited by Mike Shipston

Cellular quiescence, a reversible state in which growth, proliferation, and other cellular activities are arrested, is important for self-renewal, differentiation, development, regeneration, and stress resistance. However, the physiological mechanisms underlying cellular quiescence remain largely unknown. In the present study, we used embryos of the crustacean *Artemia* in the diapause stage, in which these embryos remain quiescent for prolonged periods, as a model to explore the relationship between cell-membrane potential (V_{mem}) and quiescence. We found that V_{mem} is hyperpolarized and that the intracellular chloride concentration is high in diapause embryos, whereas V_{mem} is depolarized and intracellular chloride concentration is reduced in postdiapause embryos and during further embryonic development. We identified and characterized the chloride ion channel protein cystic fibrosis transmembrane conductance regulator (CFTR) of *Artemia* (*Ar*-CFTR) and found that its expression is silenced in quiescent cells of *Artemia* diapause embryos but remains constant in all other embryonic stages. *Ar*-CFTR knockdown and GlyH-101–mediated chemical inhibition of *Ar*-CFTR produced diapause embryos having a high V_{mem} and intracellular chloride concentration, whereas control *Artemia* embryos released free-swimming nauplius larvae. Transcriptome analysis of embryos at different developmental stages revealed that proliferation, differentiation, and metabolism are suppressed in diapause embryos and restored in postdiapause embryos. Combined with RNA sequencing (RNA-Seq) of GlyH-101–treated MCF-7 breast cancer cells, these analyses revealed that CFTR inhibition down-regulates the Wnt and Aurora Kinase A (AURKA) signaling pathways and up-regulates the p53 signaling pathway. Our findings provide insight into CFTR-mediated regulation of cellular quiescence and V_{mem} in the *Artemia* model.

Cellular quiescence is a sleep-like and reversible state in which growth, proliferation, and other cellular activities are arrested. This state is thought to be homogenous and induced by diverse anti-mitogenic signals (1). Quiescent cells re-enter the cell cycle in response to physiological stimuli (2). Reactivation of quiescent cells is crucial for tissue repair and regeneration and plays a key role in growth, development, and health of higher multicellular organisms (3–5). Cellular quiescence also explains how some species produce embryos in a state of diapause or dormancy, which often enables their offspring to survive remarkably harsh environmental conditions (6, 7). Development, reproduction, and metabolic activities are highly suppressed in this state, meaning that embryos are protected until the environmental conditions become favorable, at which point the cell cycle resumes (8). Entry of cells into quiescence is often associated with dramatic changes in metabolism (9) and cell-cycle regulation. In addition, the cell membrane potential (V_{mem}) becomes hyperpolarized (10, 11). V_{mem}, which refers to the voltage across the plasma membrane, is a key bioelectric property of nonexcitable cells (12). Hyperpolarization of the resting V_{mem} is accompanied by decreased proliferation of astrocytes isolated from the developing spinal cord and hippocampus of rats (13, 14). These observations led us to speculate that V_{mem} plays a critical role in cellular quiescence. However, there have been few reports on the relationship between cellular quiescence and V_{mem}.

Ion channels establish the resting V_{mem} of all cells by determining the gradients of major ions, such as sodium, potassium, calcium, and chloride, across the cell membrane (15). Chloride, which is the most abundant anion in all organisms, has multiple functions, including regulation of cell volume, signal transduction, cell death/survival, and intracellular pH and is believed to contribute to V_{mem} (16, 17). Cystic fibrosis transmembrane

This work was supported by National Major Research and Development Projects of China Grant 2016YFA0101201 and National Natural Science Foundation of China Grants 31730084 and 41711530710. The authors declare that they have no conflicts of interest with the contents of this article.

This article contains Tables S1 and S2 and Figs. S1–S12.

The nucleotide sequence(s) reported in this paper has been submitted to the DDBJ/GenBank™/EBI Data Bank with accession number(s) MH822146.

The data discussed in this publication have been deposited in NCBI's Gene Expression Omnibus and are accessible through GEO Series accession number GSE124776.

[1] To whom correspondence should be addressed: College of Life Sciences, Zhejiang University, Hangzhou, Zhejiang 310058, China. Tel./Fax: 86-571-88273176; E-mail: w_jyang@zju.edu.cn.

conductance regulator (CFTR)[2] is an ATP-gated chloride channel belonging to the ABC transporter superfamily (18). CFTR provides a pathway for reversible chloridion movement across cell membrane and regulates the rate of chloridion flow (18). Structural studies described that CFTR is composed of a regulatory R domain and two repeated domains, each of which consists of a hydrophobic membrane-spanning domain (MSD) and a cytosolic hydrophilic region for binding to ATP (NBD) (19). Increasing evidence indicates that CFTR not only is a secretory chloride channel but also modulates a wide range of other membrane transport proteins, including epithelial Na^+ channels (ENaCs), Ca^{2+}-activated chloride channels, outwardly rectifying chloride channels, and the anion (Cl^-/HCO_3^-) exchanger (20–23). Mutations of the *CFTR* gene affecting its chloride channel function can lead to dysregulated fluid transport in the pancreas, lung, liver, and other organs, resulting in cystic fibrosis (24–26).

In this study, we used *Artemia*, a small crustacean, as a model system to investigate regulation of cellular quiescence. *Artemia* produce encysted gastrula embryos that rapidly enter a state of dormancy, called diapause, when environmental conditions are unfavorable (27, 28). A number of cross-sectional studies suggest an association between *Artemia* and dormancy (29–34).

The present study demonstrates that V_{mem} was hyperpolarized and the intracellular chloride concentration was high in diapause embryos, whereas V_{mem} was depolarized and the intracellular chloride concentration was reduced in postdiapause embryos and during further embryonic development. CFTR of *Artemia* (*Ar*-CFTR) was silenced in diapause embryos, leading to inhibition of chloride outflow and consequently hyperpolarization. Transcriptome analysis indicated that proliferation, differentiation, and metabolism were suppressed in diapause embryos and that the Wnt and AURKA signaling pathways were down-regulated and the p53 signaling pathway was up-regulated upon inhibition of CFTR. Our findings provide evidence that modulation of V_{mem} by CFTR regulates cellular quiescence.

Results

Cells in Artemia diapause embryos are quiescent and hyperpolarized

Artemia possesses two independent reproductive pathways, ovoviviparous and oviparous, as a strategy to survive fluctuating environmental conditions. Under favorable conditions, embryos mature in the ovisac (uterus) and are released into the environment as free-swimming nauplius larvae via the ovoviviparous pathway (Fig. 1*A*, *panels 1* and *2*). By contrast, under unfavorable conditions, mature females produce and release encysted embryos that exist in a state of obligate dormancy, called diapause, via the oviparous pathway (Fig. 1*A*, *panels 3* and *4*). Cells in diapause embryos can remain quiescent and not divide for many years (27). Signals received from favorable environmental stimuli terminate diapause. This induces embryos to enter a state, followed by hatching of swimming nauplii after 18–24 h (Fig. 1*A*, *panels 5–7*). Western blotting analysis showed that expression of cell proliferation markers, phosphorylation histone H3 at Ser^{10} (pH3S10) and phosphorylation of retinoblastoma at Thr^{356} (pRbT356), was greatly reduced in diapause and postdiapause embryos (Fig. 1*B*). This finding suggests that the cell cycle has ceased at the diapause and postdiapause stages but not at other developmental stages. Furthermore, immunofluorescence analysis showed that the proliferation markers Ki67 and proliferating cell nuclear antigen (PCNA) were expressed in postdiapause embryos but not in diapause embryos (Fig. 1*C*). These results indicate that cells are quiescent in *Artemia* diapause embryos.

This study focused on V_{mem} in *Artemia* during diapause formation. We isolated cells from embryos at each developmental stage (Fig. S1) and measured V_{mem} using $DiBAC_4(3)$, a V_{mem}-sensitive dye (Fig. 1*D*). Cells were considered depolarized when V_{mem} became less negative and hyperpolarized when V_{mem} became more negative. V_{mem} was relatively constant during ovoviviparous development; however, cells were extremely hyperpolarized from the prediapause stage to the diapause stage and depolarized in the postdiapause and nauplii stages.

We measured the intracellular chloride concentration at each developmental stage using MQAE, a chloride-sensitive fluorescent dye. The fluorescence intensity of this dye decreases as the intracellular chloride concentration increases. Almost no fluorescence was observed in cells of diapause embryos (Fig. 1*E*), indicating that the intracellular chloride concentration was high. Taken together, these results indicate that cells in diapause embryos are quiescent and hyperpolarized with a high intracellular chloride concentration.

Identification and characterization of Ar-CFTR

To investigate the regulation of V_{mem} during diapause formation, we characterized *Ar*-CFTR. A candidate for *Ar-CFTR* was identified using the tblastn algorithm with human *CFTR* as the input. The full-length *Ar-CFTR* mRNA is 4924 bp, with a 4635-bp ORF encoding a protein of 1545 amino acids (aa) (Fig. S2). The calculated molecular mass and pI of *Ar*-CFTR are 173.02 kDa and 7.43, respectively. Structure analysis showed that *Ar*-CFTR contains two MSDs, MSD1 (aa 316–581) and MSD2 (aa 981–1255); two nucleotide-binding domains, NBD1 (aa 625–825) and NBD2 (aa 1302–1522); and a regulatory domain, R (aa 638–963), which are conserved in typical CFTRs (Fig. S3*A*).

The amino acid sequence of the R domain of *Ar*-CFTR shows low overall sequence similarity (<30%) with those of the R domains of CFTRs in other species. However, the amino acids predicted to interact with serine and play a role in phosphorylation-dependent activation of this channel *in vivo* are conserved in *Ar*-CFTR, including Ser^{686}, Ser^{700}, Ser^{712}, Ser^{737}, and Ser^{768} in the KXS/RXXS motif (Fig. S3*B*). Phylogenetic analysis

[2] The abbreviations used are: CFTR, cystic fibrosis transmembrane conductance regulator; pH3S10, phosphorylation histone H3 at Ser^{10}; pRbT356, phosphorylation of retinoblastoma at Thr^{356}; MSD, membrane-spanning domain; NBD, nucleotide-binding domain; R domain, regulatory domain; GO, Gene Ontology; DEG, differentially expressed genes; ENaC, epithelial Na^+ channel; PCNA, proliferating cell nuclear antigen; MQAE, *N*-[ethoxycarbonylme-thyl]-6-methoxy-quino-linium bromide; aa, amino acid(s); qPCR, quantitative PCR; DEG, differentially expressed gene; PLK, Polo-like kinase; MEK, mitogen-activated protein kinase/extracellular signal-regulated kinase kinase ERK, extracellular signal-regulated kinase; AMPK, AMP-activated protein kinase; DAPI, 4′,6-diamidino-2-phenylindole; EdU, 5-ethynyl-2′-deoxyuridine $DiBAC_4(3)$, bis-[1,3-dibutylbarbituric] acid trimethin eoxonol; RNA-Seq, RNA sequencing; AURKA, aurora kinase A; RSK, ribosomal S6 kinase; DVL, dishevelled; TCF, transcription factor; LKB1, liver kinase B1; EMEM, eagle's minimum essential medium.

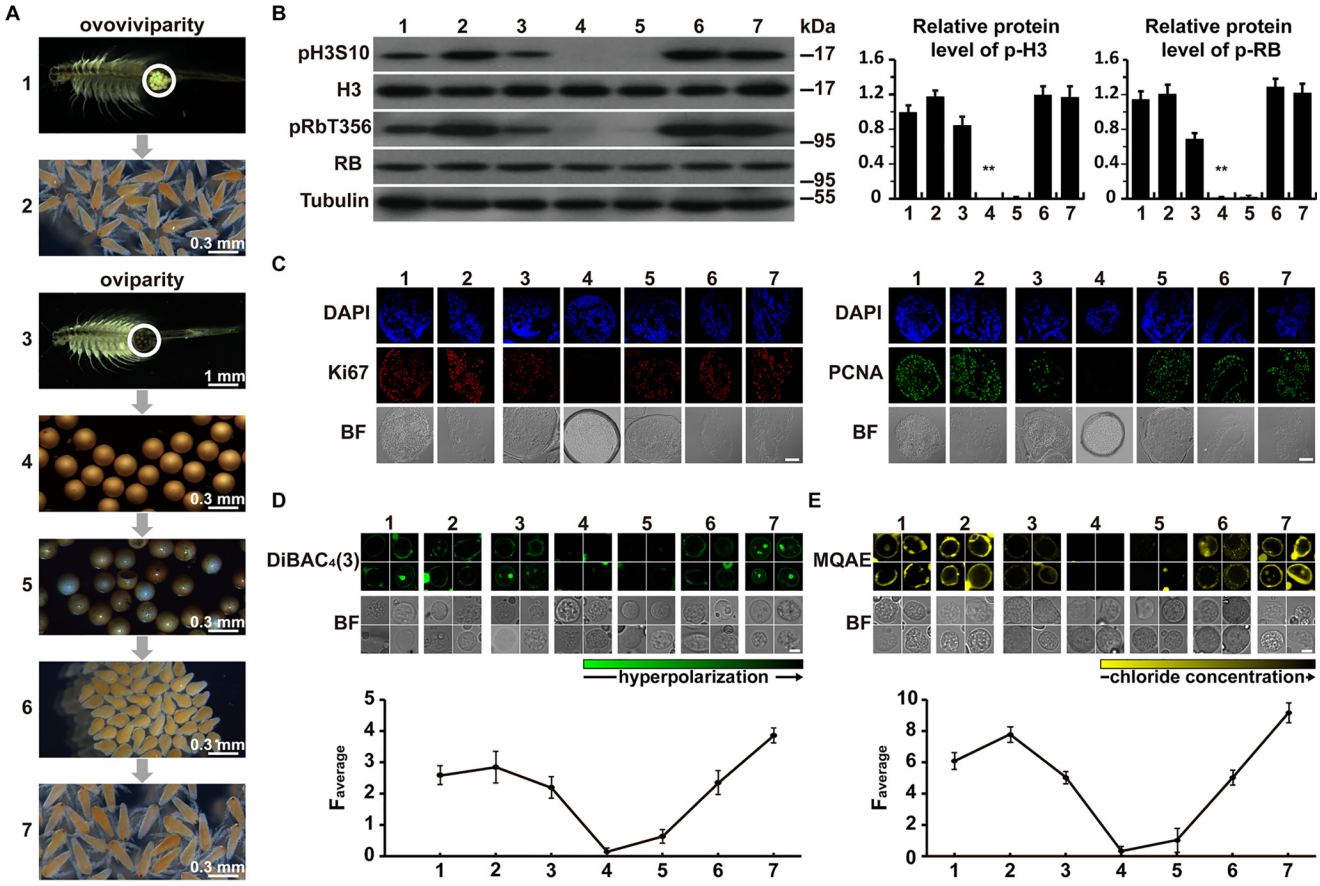

Figure 1. Cellular quiescence, V_{mem}, and the intracellular chloride concentration during diapause formation and termination in *Artemia*. *A*, various stages of the two reproductive pathways of *Artemia*. *Panel 1*, nauplius-destined ovoviviparous embryos are in the ovisac ($n = 15$ ovisacs); *panel 2*, swimming nauplii ($n = 100$ nauplii); *panel 3*, diapause-destined oviparous embryos are in the ovisac (prediapause) ($n = 15$ ovisacs); *panel 4*, diapause embryos ($n = 100$ embryos); *panel 5*, postdiapause embryos ($n = 100$ embryos); *panel 6*, 12 h of hatching of postdiapause embryos ($n = 100$ embryos); *panel 7*, 24 h of hatching of postdiapause embryos ($n = 100$ nauplii). *White circles* indicate ovisacs. *B*, Western blotting analysis of pH3S10 and pRbT356 at each developmental stage. Tubulin was used as a loading control. Relative band intensities were quantified using ImageJ. **, $p \leq 0.01$. *C*, immunofluorescence analysis of Ki67 and PCNA at each developmental stage. DAPI is counterstained with nuclei. *Bars*, 50 μm. *D*, V_{mem} of cells at each developmental stage. *Bar*, 5 μm. The average fluorescence intensity ($F_{average}$) was quantified (*bottom panel*) ($n = 15$ cells). The *color bar* indicates the relative level of hyperpolarization. *E*, intracellular chloride concentration at each developmental stage. The average fluorescence intensity ($F_{average}$) was quantified (*bottom panel*) ($n = 15$ cells). The *color bar* indicates the relative level of chloride concentration. *Bar*, 5 μm. *BF*, brightfield.

suggested that *Ar*-CFTR is grouped with CFTR expressed in the arthropod *Daphnia pulex* (Fig. S3*C*).

Polyclonal antibodies specific to *Ar*-CFTR detected a band of ~173 kDa in *Artemia*. The mRNA level of *Ar-CFTR* at each developmental stage was analyzed by real-time quantitative PCR (qPCR). mRNA expression of *Ar-CFTR* was ~2–4-fold lower in diapause embryos than in embryos at other stages of the ovoviviparous pathway (Fig. 2*A*). Similarly, protein expression of *Ar*-CFTR was ~7–10-fold lower in diapause embryos than in embryos at other developmental stages according to analysis performed using ImageJ (Fig. 2*B*). Furthermore, immunofluorescence analysis showed that *Ar*-CFTR was barely detected in diapause embryos but was observed at the cellular membrane in prediapause embryos, postdiapause embryos, and hatched nauplii (Fig. 2*C*). Thus, down-regulation of *Ar*-CFTR may be important for cellular quiescence during diapause formation in *Artemia*.

Ar-CFTR plays a critical role in regulation of cellular quiescence and diapause formation by modulating V_{mem}

To elucidate the role of *Ar*-CFTR in the regulation of diapause formation in *Artemia*, *Ar-CFTR* was knocked down by RNAi. A dsRNA designed based on the *Ar-CFTR* cDNA sequence was injected prior to ovarian development. Real-time qPCR and Western blotting analyses revealed that the mRNA and protein levels of *Ar*-CFTR were more than 80% lower in animals injected with *Ar-CFTR* dsRNA (*Ar*-CFTRi) than in those injected with *GFP* dsRNA (GFPi) (Fig. 3, *A* and *B*). An average of 75% of ovoviviparous *Artemia* injected with *Ar-CFTR* dsRNA released diapause embryos, whereas all of those injected with *GFP* dsRNA produced free-swimming nauplii (Fig. 3*C*). Western blotting and immunofluorescence analyses showed that expression of pH3S10, pRbT356, Ki67, and PCNA was reduced upon *Ar-CFTR* knockdown (Fig. 3, *D* and *E*). Furthermore, the diapause-specific proteins p26 and artemin (35, 36) were enriched upon *Ar-CFTR* knockdown (Fig. 3*D*).

Next, we investigated whether knockdown of *Ar-CFTR* induces hyperpolarization by increasing the intracellular chloride concentration. As expected, analysis of the fluorescence intensity of MQAE showed that *Ar-CFTR* knockdown increased the intracellular chloride concentration (Fig. 3*F*). Moreover, the fluorescence intensity of $DiBAC_4(3)$ was mark-

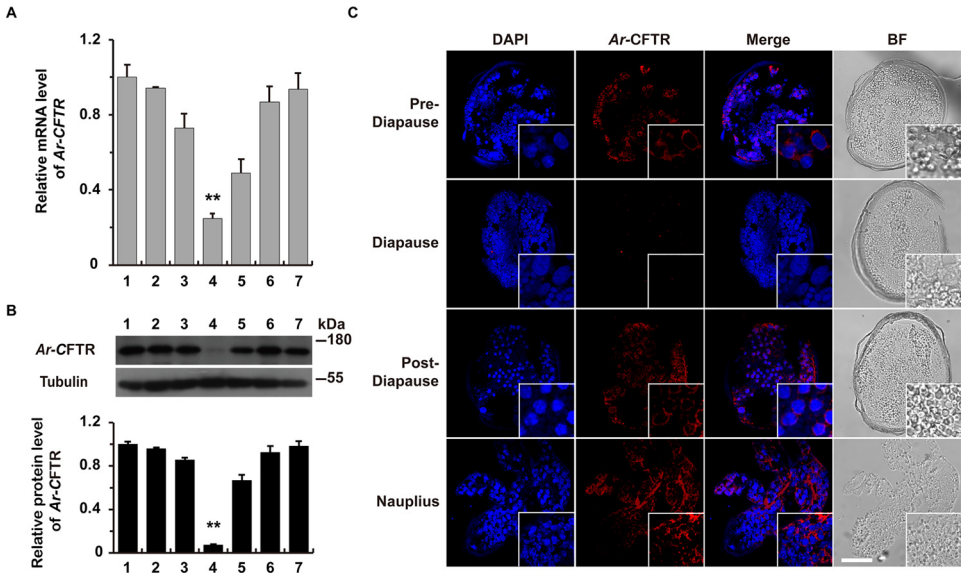

Figure 2. Molecular characterization and expression pattern of *Ar*-CFTR during development. *A*, real-time qPCR analysis of *Ar-CFTR* mRNA expression at each developmental stage (numbers indicated in Fig. 1*A* legend). mRNA expression of *Ar-CFTR* was normalized against that of *tubulin*. **, $p \leq 0.01$. *B*, Western blotting analysis of *Ar*-CFTR protein expression at each developmental stage. Tubulin was used as a loading control. Relative band intensities were quantified using ImageJ. **, $p \leq 0.01$. *C*, immunofluorescence analysis of *Ar*-CFTR at each developmental stage. *Bar*, 50 μm. *BF*, brightfield.

edly reduced upon *Ar-CFTR* knockdown (Fig. 3*G*), indicating that silencing of *Ar*-CFTR induces hyperpolarization.

To further verify the function of *Ar*-CFTR, we soaked nauplius-destined *Artemia* adults in 40‰ seawater containing 30 μM GlyH-101, a CFTR inhibitor. 30 μM was chosen according to a result of a dose-dependent experiment (Fig. S4*A*). Average 85% of ovoviviparous *Artemia* adults treated with GlyH-101 produced diapause embryos, whereas control *Artemia* adults treated with 30 μM DMSO released nauplii (Fig. 4*A*). Analysis of the chloride concentration and V_{mem} showed that inhibition of *Ar*-CFTR by GlyH-101 induced hyperpolarization by preventing chloride outflow (Fig. 4, *B* and *C*). The induced hyperpolarization was validated by analysis of a patch clamp recording (Fig. S5). Inhibition of *Ar*-CFTR by GlyH-101 also decreased the intracellular potassium and sodium concentrations, which were lower in diapause embryos than in prediapause and postdiapause embryos (Fig. S6). These findings indicate that CFTR regulates V_{mem} and thereby controls cellular quiescence during diapause formation. In addition, GlyH-101 treatment decreased expression of pH3S10, pRbT356, Ki67, and PCNA but increased that of p26 and artemin (Fig. 4, *D* and *E*).

To investigate the function of *Ar*-CFTR in termination of cellular quiescence in diapause embryos, we treated decapsulated postdiapause embryos with 100 μM GlyH-101 to suppress *Ar*-CFTR activity during hatching. 100 μM was chosen according to the results of a dose-dependent experiment (Fig. S4*B*). Development of GlyH-101–treated embryos was arrested at the pre-emergence stage, before resumption of cell division (Fig. 5*A*). However, swimming nauplii hatched from control postdiapause embryos treated with DMSO after 24 h. In addition, removal of GlyH-101 resulted in average of 80% released nauplii, a rate that is similar to the natural hatching rate of *Artemia* in its natural environment (Fig. 5*A*). The results indicated that *Ar*-CFTR is required for termination of cellular quiescence. Fluorescence analysis using the bioelectricity reporter $DiBAC_4(3)$ and the chloride-sensitive dye MQAE revealed that V_{mem} remained hyperpolarized, and the chloride concentration remained high upon continuous treatment with GlyH-101 (Fig. 5, *B* and *C*). However, V_{mem} was depolarized, and chloride outflow was increased following removal of GlyH-101 (Fig. 5, *B* and *C*). Western blotting analysis revealed that levels of pH3S10 and pRbT356 increased after the pre-emergence stage and were high in nauplii in the control group. However, the levels of these two proliferation markers were low in the presence of GlyH-101 and increased after removal of GlyH-101 (Fig. 5*D*). Together, these results indicate that *Ar*-CFTR controls cellular quiescence during diapause formation by mediating chloride outflow and thereby modulating V_{mem}.

Molecular signatures of quiescent cells in diapause embryos

To characterize the molecular signatures of quiescent cells and analyze downstream signaling pathways of CFTR, RNA-Seq of diapause embryos was performed. Genes that were differentially expressed between nauplius-destined ovoviviparous embryos, diapause-destined oviparous embryos (prediapause), diapause embryos, and postdiapause embryos are presented in a heat map (Fig. 6*A*). In total, 9573, 9458, and 6356 genes were differentially expressed between nauplius-destined ovoviviparous embryos and diapause embryos, between prediapause and diapause embryos, and between postdiapause and diapause embryos, respectively (Fig. 6*B*). In addition, expression of 3167 genes, including markers of diapause (p26, artemin, and ArHsp22) and cell division (Ki67 and PCNA), was higher or lower in diapause embryos than in ovoviviparous, prediapause, and postdiapause embryos. These results reveal the key molecular characteristics of quiescent cells in diapause embryos. Gene ontology (GO) enrichment analysis was performed of genes that were differentially expressed between diapause and postdiapause embryos. This revealed that expression of genes associated with proliferation, differentiation, and metabolism

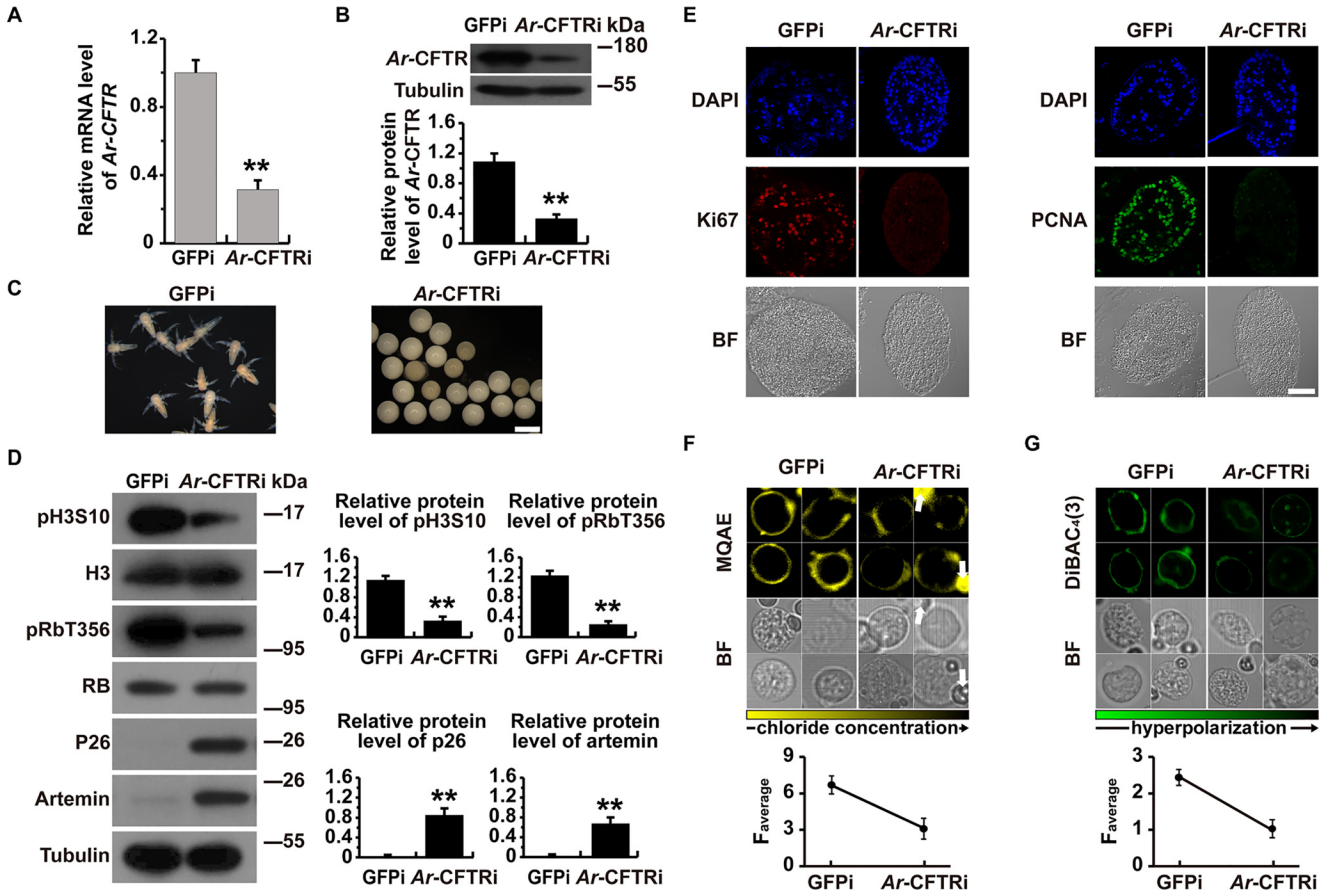

Figure 3. Knockdown of *Ar*-CFTR in developing embryos. *A*, real-time qPCR analysis of *Ar-CFTR* mRNA expression upon injection of *Ar*-CFTR and GFP dsRNAs. **, $p \leq 0.01$. *B*, Western blotting analysis of *Ar*-CFTR protein expression upon injection of *Ar*-CFTR and GFP dsRNAs. Tubulin was used as a loading control. Relative band intensities were quantified using ImageJ. **, $p \leq 0.01$. *C*, phenotypes of diapause embryos produced by ovoviviparous *Artemia* injected with *Ar-CFTR* dsRNA and of nauplii produced by ovoviviparous *Artemia* injected with GFP dsRNA. *Bar*, 0.2 mm. *D*, Western blotting analysis of pH3S10, pRbT356, and the diapause-specific proteins p26 and artemin upon injection of *Ar*-CFTR and GFP dsRNAs. Tubulin was used as a loading control. Relative band intensities were quantified using ImageJ. **, $p \leq 0.01$. *E*, immunofluorescence analysis of Ki67 and PCNA upon injection of *Ar*-CFTR and GFP dsRNAs. *Bar*, 50 μm. *F*, intracellular chloride concentration upon injection of *Ar*-CFTR and GFP dsRNAs. *White arrows* indicate lipid droplets. The average fluorescence intensity ($F_{average}$) was quantified (*bottom panel*) ($n = 15$ cells). The *color bar* indicates the relative level of chloride concentration. *Bar*, 5 μm. *G*, V_{mem} upon injection of *Ar*-CFTR and GFP dsRNAs. The average fluorescence intensity ($F_{average}$) was quantified (*bottom panel*) ($n = 15$ cells). The *color bar* indicates the relative level of hyperpolarization. *Bar*, 5 μm. *BF*, brightfield. $n = 40$ *Artemia* adults injected with dsRNA.

was suppressed in diapause embryos (Fig. 6*C*). Genes related to metabolism, including those associated with oxidative phosphorylation, the carbohydrate metabolic process, the cholesterol metabolic process, polysaccharide digestion, the fatty–acyl-CoA metabolic process, the aerobic electron transport chain, and autophagy, as well as genes related to cell proliferation, including those associated with the mitotic cell cycle, RNA polymerase II transcription factor activity, and translation regulator activity, were down-regulated in diapause embryos. By contrast, genes associated with chitin binding, cuticle development, negative regulation of cellular metabolic processes, and lipid storage were up-regulated in diapause embryos. Analysis of related pathways and genes showed that the Wnt and AURKA signaling pathways were down-regulated, and the p53 signaling pathway was up-regulated in diapause embryos (Fig. S7).

Pathways upstream and downstream of CFTR-regulated hyperpolarization in MCF-7 cells

To identify the signaling pathways by which CFTR-regulated hyperpolarization controls cellular quiescence, we treated MCF-7 cells with 10 μM GlyH-101 to inhibit CFTR. 10 μM was chosen according to a result of a dose-dependent experiment (Fig. S4*C*). Immunofluorescence analysis of the proliferation marker Ki67, EdU incorporation analysis, and Western blotting analysis of pH3S10 and pRbT356 indicated that GlyH-101–treated cells lacked mitotic activity, in contrast to control cells, and that mitotic activity was restored after removal of GlyH-101 (Fig. 7*A*). Cells in different phases of the cell cycle were distinguished by flow cytometric analysis. After treatment with GlyH-101 for 24 h, the percentage of G_0/G_1 phase cells increased from 56.95 to 69.03%. These changes reverted to the original state after the removal of GlyH-101 (Fig. 7*B*). Similar to the results obtained in *Artemia*, the fluorescence intensity of MQAE was decreased in GlyH-101–treated cells, indicating that inhibition of CFTR increases the intracellular chloride concentration, and returned to normal after removal of GlyH-101 (Fig. 7*C*). In addition, we monitored the effects of CFTR inhibition on V_{mem}. GlyH-101 treatment immediately and markedly decreased the fluorescence intensity of $DiBAC_4(3)$ (Fig. 7*D*). The dynamic patterns of intracellular chloride concentration and V_{mem} are shown in Fig. S8. The mean resting

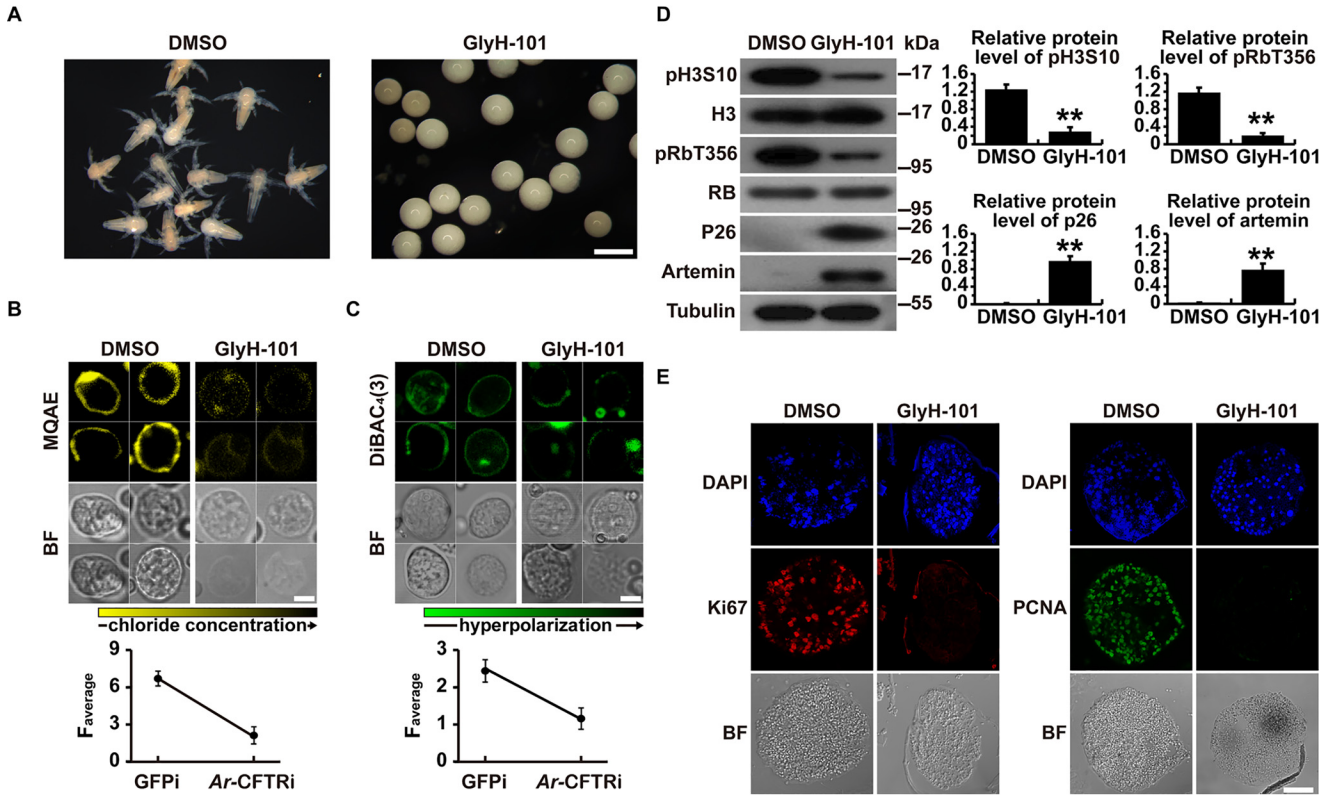

Figure 4. Suppression of *Ar*-CFTR activity in developing embryos. *A*, phenotypes of diapause embryos produced by ovoviviparous *Artemia* treated with GlyH-101 and of nauplii produced by ovoviviparous *Artemia* treated with DMSO. *Bar*, 0.2 mm. *B*, intracellular chloride concentration upon treatment with GlyH-101 and DMSO. The average fluorescence intensity ($F_{average}$) was quantified (*bottom panel*) ($n = 15$ cells). The *color bar* indicates the relative level of chloride concentration. *Bar*, 5 μm. *C*, V_{mem} upon treatment with GlyH-101 and DMSO. The average fluorescence intensity ($F_{average}$) was quantified (*bottom panel*) ($n = 15$ cells). The *color bar* indicates the relative level of hyperpolarization. *Bar*, 5 μm. *D*, Western blotting analysis of pH3S10, pRbT356, and the diapause-specific proteins p26 and artemin upon treatment with GlyH-101 and DMSO. Tubulin was used as a loading control. Relative band intensities were quantified using ImageJ. **, $p \leq 0.01$. *E*, immunofluorescence analysis of Ki67 and PCNA upon treatment with GlyH-101 and DMSO. *Bar*, 50 μm. *BF*, brightfield. $n = 40$ *Artemia* adults soaked with DMSO or GlyH-101.

V_{mem} was patched in the whole-cell configuration and ranged from −46 to −94 mV after treatment with GlyH-101 for 24 h and returned to −42 mV following removal of GlyH-101 (Fig. 7*E*). The patch clamp tracing also showed that GlyH-101 inhibited the chloride currents in MCF-7 cells (Fig. S9). In contrast to MCF-7 cell line, after GlyH-101 treatment, the hyperpolarization and proliferation inhibition were not observed in the U251 cell line (which has an extremely low level of CFTR expression) (Fig. S10). In addition, *CFTR* knockdown in SKOV3 and HT-29 could induce cellular quiescence in the both of these cell lines (Fig. S11). The results may indicate that inhibition of CFTR leads to hyperpolarization, a high intracellular chloride concentration, and quiescence in mammalian cells.

To interrogate the pathways downstream of CFTR-regulated hyperpolarization in quiescent cells, RNA-Seq of GlyH-101–treated MCF-7 cells was performed. The transcriptome profiles of three replicates of MCF-7 cells treated with GlyH-101 for 0, 1, and 24 h were compared. We performed cluster analysis of differentially expressed genes (DEGs) in the entire transcriptome and observed the overall expression gene pattern in GlyH-101–treated cells. The gene expression pattern markedly differed between cells treated with GlyH-101 for 24 h and untreated cells (Fig. S12). In total, 2749 genes were differentially expressed between cells treated with GlyH-101 for 1 h and untreated cells, whereas 8021 genes were differentially expressed between cells treated with GlyH-101 for 24 h and untreated cells (Fig. 8*A*). According to ranking of the fold changes in gene expression and analysis of the gene signatures of quiescent cells in the molecular function, metabolic processes, and pathways categories, 31 typical DEGs were identified (Fig. 8*B* and Table S1). GO enrichment analysis of DEGs is shown in Fig. 8*C*. Genes involved in the p53 signaling pathway and negative regulation of cell proliferation were up-regulated in cells treated with GlyH-101 for 24 h, whereas genes involved in cell division, the Wnt and AURKA signaling pathways, and many metabolic pathways were down-regulated. The analysis of transcriptomes in *Artemia* diapause and GlyH-101–treated MCF-7 cells showed some similar signatures of cellular quiescence based on GO term enrichment, including the genes of p53 and Wnt signaling pathways (Fig. S13). Our results demonstrate that CFTR may regulates V_{mem} and cellular quiescence in both *Artemia* and MCF-7 cells.

Discussion

Artemia is an ideal model system to study the regulation of cellular quiescence because embryos can remain in diapause for prolonged periods, and the cell cycle resumes during development of postdiapause embryos. The present study demonstrates that V_{mem} was hyperpolarized and the intracellular chloride concentration was high in diapause embryos and that

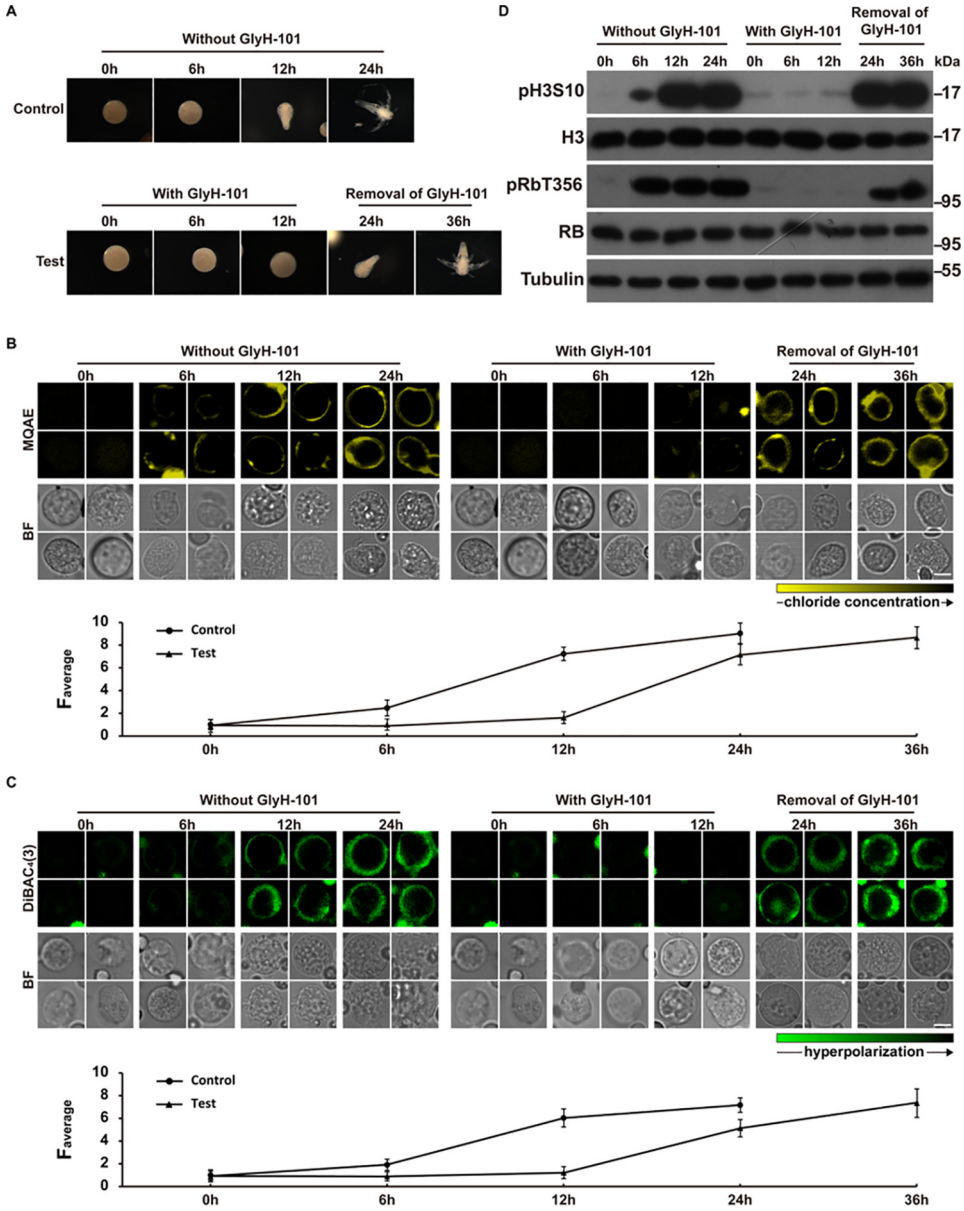

Figure 5. Suppression of *Ar*-CFTR activity during postdiapause development. *A*, phenotypes of control and GlyH-101–treated embryos. *Bar*, 0.2 mm. *Control*, 0–24 h, 20‰ seawater containing DMSO. *Test*, 0–12 h, 20‰ seawater containing GlyH-101; 24–36 h, removal of GlyH-101 after 12 h. *B*, intracellular chloride concentration in control and test samples at the indicated time points. The average fluorescence intensity ($F_{average}$) was quantified (*bottom panel*) (n = 15 cells). The *color bar* indicates the relative level of chloride concentration. *Bar*, 5 μm. *C*, V_{mem} in control and test samples at the indicated time points. *Bar*, 5 μm. The average fluorescence intensity ($F_{average}$) was quantified (*bottom panel*) (n = 15 cells). The *color bar* indicates the relative level of hyperpolarization. *D*, Western blotting analysis of pH3S10 and pRbT356 in control and test samples at the indicated time points. Tubulin was used as a loading control. Relative band intensities were quantified using ImageJ. **, $p \leq 0.01$. *BF*, brightfield. n = 100 embryos soaked with DMSO or GlyH-101.

this was controlled by *Ar*-CFTR. Thus, *Ar*-CFTR–regulated hyperpolarization seems required for cellular quiescence during diapause formation in *Artemia*. Transcriptome analysis indicated that proliferation, differentiation, and metabolism were suppressed, the Wnt and AURKA signaling pathways were down-regulated, and the p53 signaling pathway was up-regulated in diapause embryos and GlyH-101–treated MCF-7 cells.

A hyperpolarized V_{mem} tends to be quiescent and does not typically undergo mitosis; conversely, a depolarized V_{mem} tends to have mitotically active (14, 37, 38). Here, V_{mem} was low in prediapause embryos (mitotic cells), hyperpolarized in diapause embryos (quiescent cells), and depolarized in postdiapause embryos and hatched nauplii (mitotic cells). This implies that hyperpolarization induces cellular quiescence during diapause formation in *Artemia*.

Fluctuations in the chloride concentration contribute to cell polarity, and this appears to be linked to the cell cycle and regulates the proliferation of various cell types (39, 40). ClC-3, a member of the voltage-gated chloride channel protein family, modulates proliferation of rat basilar arterial smooth muscle cells by suppressing Akt/GSK-3β signaling pathway, leading to down-regulation of cyclin D1 and cyclin E (41). Furthermore, the chloride channel blocker 5-*N*-2-(3-phenylpropylamino) benzoic acid inhibits re-entry of quiescent (G_0) NIH-3T3 fibroblasts into the cell cycle (42). However, other voltage-gated ion

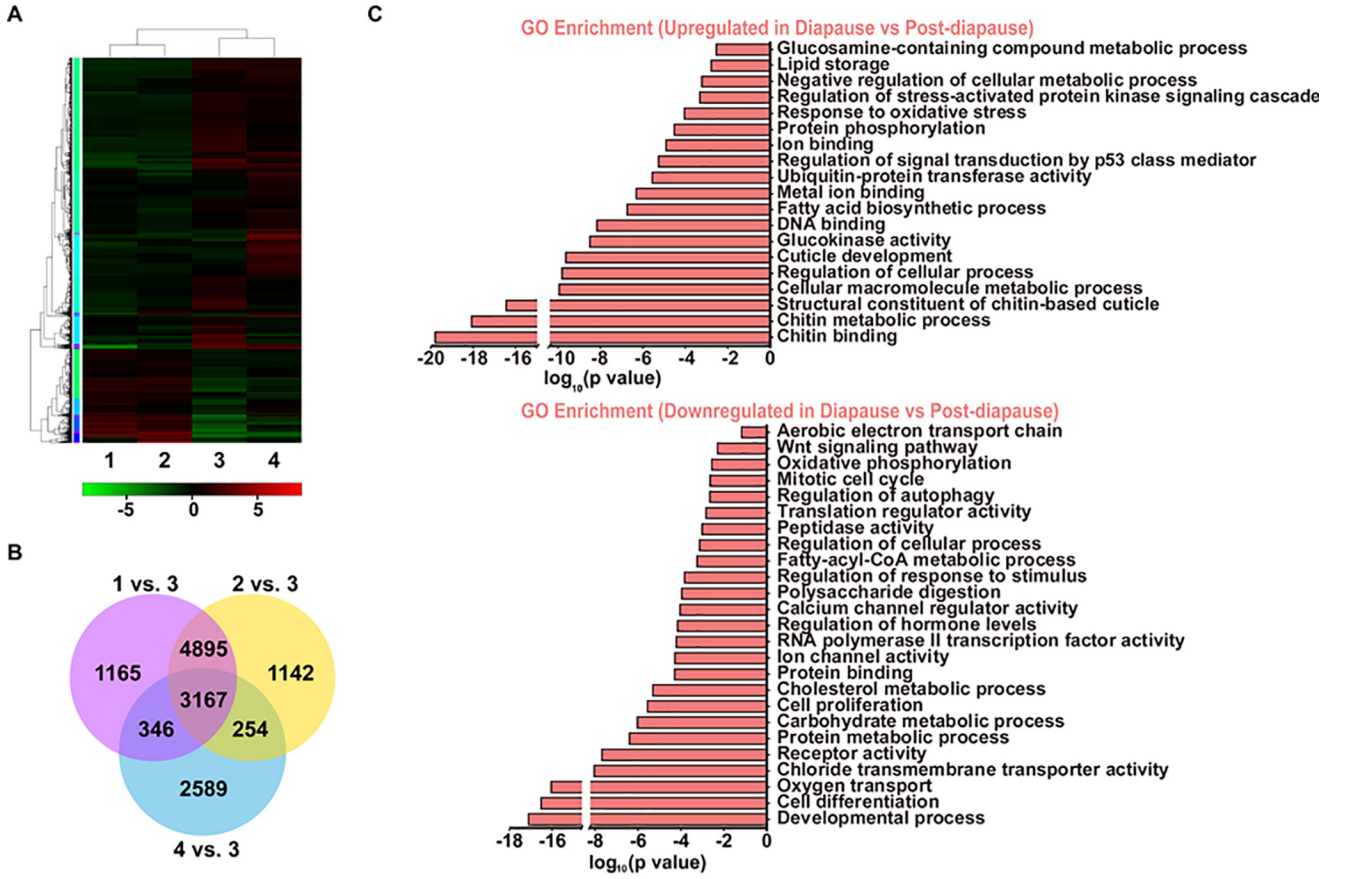

Figure 6. RNA-Seq analysis of quiescent cells in diapause embryos. *A*, cluster analysis of DEGs. *Colors* indicate log10 (TPM+1). *B*, GO enrichment analysis of up-regulated and down-regulated DEGs. *C*, Venn diagram showing the numbers of DEGs. *Group 1*, nauplius-destined ovoviviparous embryos ($n = 15$ ovisacs); *group 2*, prediapause embryos ($n = 15$ ovisacs); *group 3*, diapause embryos ($n = 100$ embryos); *group 4*, postdiapause embryos ($n = 100$ embryos). *TPM*, transcripts per million.

channels, such as potassium, calcium, and sodium channels, which contribute to hyperpolarization, also regulate cell proliferation (43–45). In neural stem cells, conditional deletion of ENaCs results in the absence of inward sodium flow, which induces hyperpolarization and reduces the number and proliferation of cells in the subependymal zone (46). An increase in potassium channel activity corresponding to transient hyperpolarization is involved in proliferation and cell cycle progression; cells reversibly arrest in G_0/G_1 phase upon inhibition of ATP-sensitive potassium channels (47, 48). Evidence has shown that CFTR affects other ion channels and ions. For example, application of a CFTR blocker was reported to reduce the inward rectifier potassium current and sodium current in the heart by ~43 and ~82% (49). CFTR inhibits ENaCs by increasing the intracellular chloride concentration in *Xenopus* oocytes (50). The inward potassium and sodium currents were decreased upon inhibition of *Ar*-CFTR by GlyH-101, and these currents were lower in diapause embryos than in prediapause and postdiapause embryos. Our results indicate that CFTR regulates the intracellular chloride concentration and influences the potassium and sodium currents and thereby modulates V_{mem} and controls cellular quiescence in *Artemia* embryos.

We previously reported that the PLK1–MEK–ERK–RSK signaling pathway regulates cellular quiescence in diapause embryos (29, 30). Here, transcriptome analysis showed that expression of AURKA, the upstream kinase of PLK1–MEK–ERK–RSK, was very low in diapause embryos, indicating that the AURKA signaling pathway was suppressed. Wnt signaling helps to maintain quiescence of hematopoietic stem cells, which may underlie why it is required to preserve the self-renewal capability of these cells (51, 52). In the current study, expression of dishevelled (DVL) and transcription factor (TCF), which are components of the Wnt signaling pathway, was significantly decreased in diapause embryos, indicating that suppression of Wnt signaling is also critical for diapause formation in *Artemia*. p53 is downstream of CFTR and plays a role in quiescence of various cell types (53). Consistently, p53 was up-regulated in diapause embryos and down-regulated in prediapause and postdiapause embryos. Moreover, liver kinase B1 (LKB1), a kinase of AMPK that is upstream of CFTR (54, 55), was highly expressed in diapause embryos, indicating that activated AMPK suppresses expression of CFTR and up-regulates expression of p53 during diapause formation in *Artemia*. Taken together, these results suggest that the AURKA–PLK–MEK–ERK–RSK, LKB1–AMPK–CFTR–p53, and Wnt signaling pathways are simultaneously required for regulation of cellular quiescence in diapause embryos.

Clinical drug therapy for cancer is far from optimal, as indicated by the high death rate of cancer patients. Standard therapies mainly target the tumor bulk but often fail to eradicate the quiescent cancer cells that may play important roles in resistance to chemoradiotherapy (56, 57). Effective targeting of the

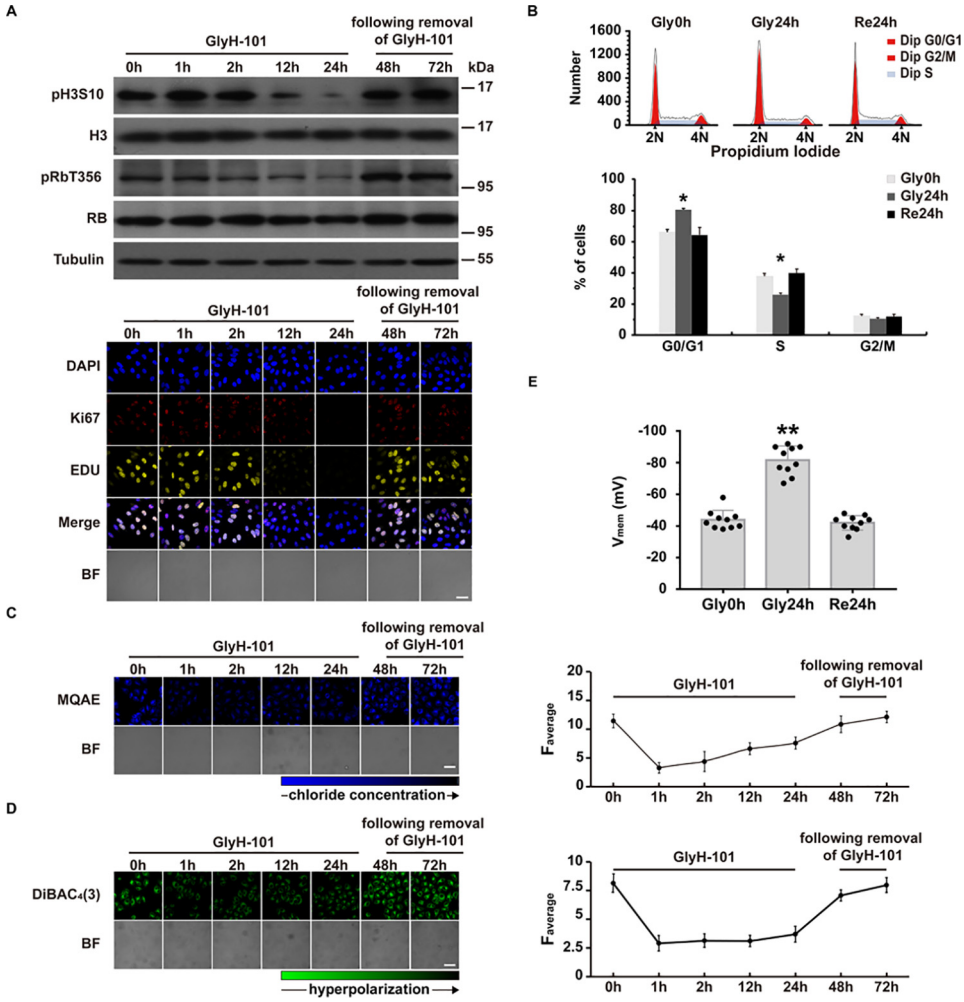

Figure 7. Inhibition of CFTR activity using GlyH-101 causes hyperpolarization and suppresses proliferation in MCF-7 cells. *A*, Western blotting analysis of pH3S10 and pRbT356 and immunofluorescence analysis of Ki67 and EDU incorporation in MCF-7 cells treated with or without GlyH-101 for the indicated durations. Tubulin was used as a loading control. *Bar*, 20 μm. *B*, flow cytometric analysis of the cell cycle. *, $p \leq 0.05$. *C*, measurement of the intracellular chloride concentration. The average fluorescence intensity ($F_{average}$) was quantified (*right panel*). The *color bar* indicates the relative level of chloride concentration. *Bar*, 20 μm. *D*, measurement of V_{mem}. The average fluorescence intensity ($F_{average}$) was quantified (*right panel*). The *color bar* indicates the relative level of hyperpolarization. *Bar*, 20 μm. *E*, whole-cell patch recording of V_{mem}. *Gly0h*, cells treated with GlyH-101 for 0 h; *Gly24h*, cells treated with GlyH-101 for 24 h; *Re24h*, cells at 24 h after removal of GlyH-101. $n = 10$ cells. **, $p \leq 0.01$. *BF*, brightfield.

quiescent cancer cells may represent a far more efficient focus toward the complete eradication of a tumor and prevention of tumor relapse. Our findings suggest that CFTR could also be used as one of the targets in the clinical treatment of cancer.

Materials and methods

Animals

Diapause cysts of parthenogenetic *Artemia* were harvested from Gahai Lake, Qinghai Province, China. Animal experiments were approved and performed in accordance with the institutional guidelines for animal care of animal ethics committee of Zhejiang University.

The cysts of parthenogenetic *Artemia* were hatched in 20‰ artificial seawater at 25 °C under continuous illumination. On the third day of the nauplii hatching from the cysts, chlorella powder (Fuqing King Dnarmsa Spirulina, China) was supplied to the seawater as food. When the nauplii developed into larvae, they were separated into two groups, one of which was reared in 40‰ artificial seawater with a photoperiod of 16 h of light and 8 h of dark per day to release the nauplii (ovoviviparity). The other group was reared in 80‰ artificial seawater with a photoperiod of 5 h of light and 19 h of dark per day to release dormant cysts (oviparity).

Western blotting analysis

Proteins were extracted using TRIzol reagent (Invitrogen). After homogenizing the sample with TRIzol™ reagent, chloroform was added, and the sample was centrifuged at 12,000 × *g* for 15 min. We then used isopropanol to precipitate proteins from the lower aqueous layer. The precipitation was washed with 0.3 M guanidine hydrochloride solution and dissolved with 2% SDS solution. Approximately 25 μg of protein from each sample was separated by 10% SDS-PAGE and transferred to P polyvinylidene difluoride membranes (Bio-Rad). Membranes were blocked for 1.5–2 h at room temperature in 5% skim milk solution and incubated with the following antibodies: anti–*Ar*-CFTR, anti-P26 and anti-Artemin were raised in rabbits (Hangzhou HuaAn Biotechnology Company, Hangzhou, China);

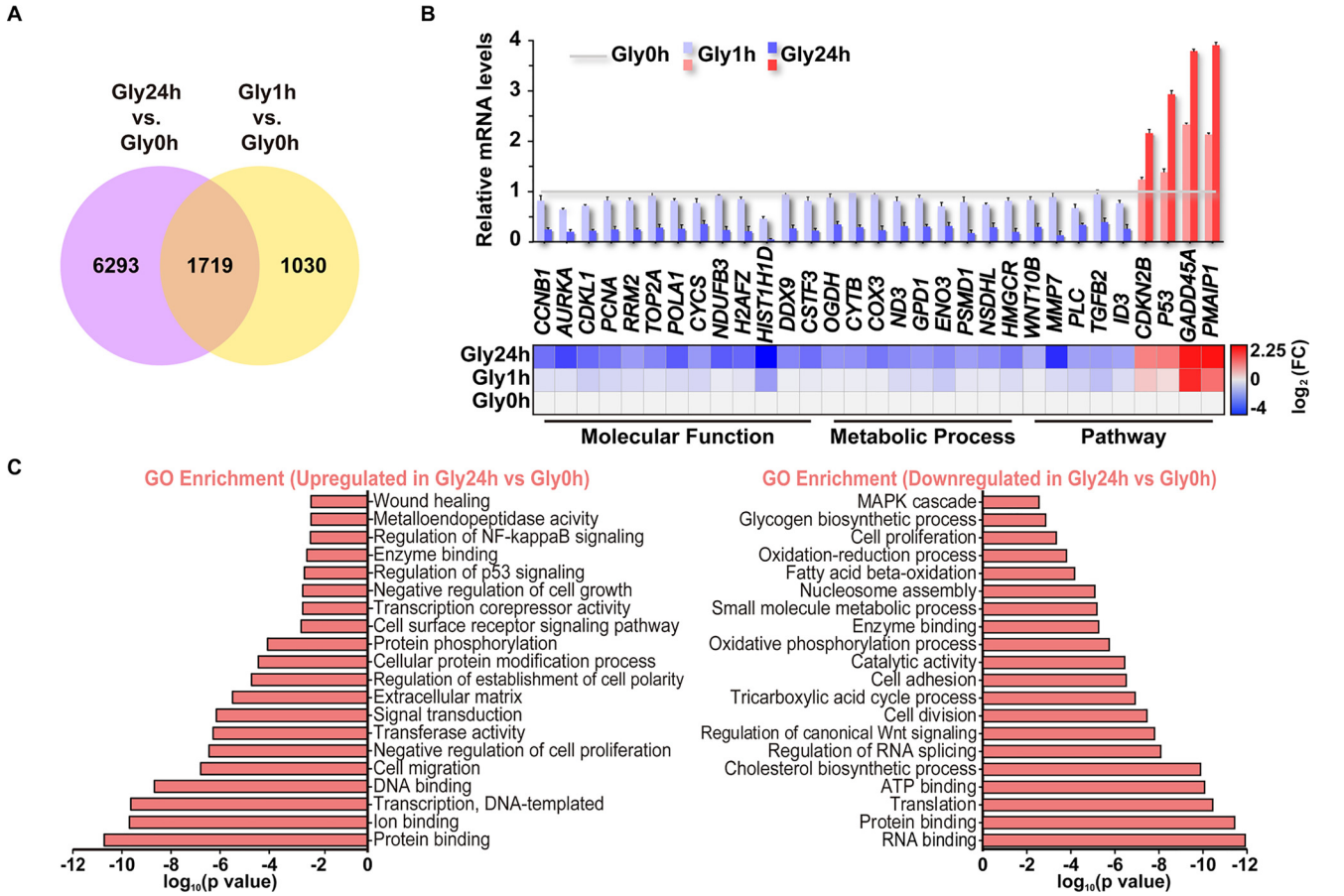

Figure 8. RNA-Seq analysis of the effect of GlyH-101 on MCF-7 cells. *A*, Venn diagram showing the number of genes that were differentially expressed between cells treated with GlyH-101 for 1 or 24 h and untreated cells. *B*, heat map and real-time qPCR analysis showing altered expression of cellular quiescence-related genes in the molecular function, metabolic process, and pathway categories in GlyH-101–treated cells. mRNA expression was normalized against that of *tubulin*. *C*, GO enrichment analysis of up-regulated and down-regulated DEGs. *Gly0h*, cells treated with GlyH-101 for 0 h; *Gly1h*, cells treated with GlyH-101 for 1 h; *Gly24h*, cells treated with GlyH-101 for 24 h. *BF*, brightfield.

anti-H3 (Cell Signaling, Boston, MA); anti-p-(Ser^{10}) H3 (Epitomics), anti-Rb (Epitomics); anti-p-(Thr^{356}) Rb (Abcam, London, UK); anti-CFTR (Abcam); and anti-tubulin-α (Sigma–Aldrich). Detection was performed using BM Chemiluminescence Western blotting kits (Roche) according to the manufacturer's instructions.

Molecular cloning of parthenogenetic Artemia CFTR cDNA

From a genomic database of *Artemia franciscana* built at Artemia Reference Center at Ghent University (Ghent, Belgium), we obtained a CFTR candidate (*Ar*-CFTR) using a homologous tblastn search with the human CFTR (GenBank^{TM} accession no. NP_000483.3) as the input. The nucleotide sequence of *Ar-CFTR* was submitted to the GenBank^{TM} under submission number MH822146. Total RNA was extracted from diapause embryos and nauplii using TRIzol reagent according to the manufacturer's instructions, 1 μg of which was used as a template to reverse-transcribe first-strand cDNA.

Phylogenetic analysis of Ar-CFTR

The evolutionary history was inferred using the Neighbor-Joining method (58). The percentages of replicate trees in which the associated taxa clustered together in the bootstrap test (1000 replicates) are shown next to the branches (59). The analysis involved 15-amino acid sequences. All positions containing gaps and missing data were eliminated. There were a total of 1247 positions in the final data set. Evolutionary analyses were conducted in MEGA7 (60).

Real-time quantitative PCR

RNA extraction and reverse-transcription were performed according to the methods mentioned above. Specific primers of *Ar*-CFTR and internal control Tubulin (RT-*Ar*-CFTR forward ATATCCCGTCAACGCTCTCAT, and RT-*Ar*-CFTR reverse TCGCTTTTCCACTTCCTTACTAC for *Ar*-CFTR; and Tubulin forward GCAGTGGTCTACAAGGTTTC and Tubulin reverse ATCAAAACGAAGGCTGGCGGTG for tubulin) were designed according to cDNA. PCRs were performed using SYBR Green (TOYOBO, Osaka, Japan) on the Bio-Rad MiniOpticon^{TM} real-time PCR system in triplicate. The list of primers used for real-time qPCR analysis of MCF-7 cells were shown in Table S2.

Statistical analysis was performed using one-way analysis of variance followed by Tukey's all pair comparison test using the STATISTICA software. Differences where the p value was equal to 0.05 were considered significant, and a p value of 0.01 was considered extremely significant. A histogram was made using the SigmaPlot 10.0 software.

Knockdown of CFTR in Artemia, SKOV3, and HT-29 cells

For dsRNA preparation, the PET-T7 plasmid containing two inverted T7 promoter sites flanking the multiple-cloning sites was used as the expression vector. To obtain the reconstructed plasmid expressing *Ar*-CFTR dsRNA, a 326-bp fragment in the coding region of the *Ar*-CFTR gene was amplified with specific primers (ds-*Ar*-CFTR forward GCTCTAGAAAATCCAAGTCTCCAAGAAAG and ds-*Ar*-CFTR reverse GGAATTCAACCCCAAAGCCCCATAA, where XbaI and EcoRI sites are underlined) and subcloned into PET-T7 at the XbaI and EcoRI sites. The recombinant plasmid was transformed into *Escherichia coli* DH5α, sequenced to confirm the inserted nucleotide sequence, and then transformed into *E. coli* HT115 cells to express the dsRNA. The plasmid expressing GFP dsRNA was constructed as described previously and was used as a negative control. The dsRNA was produced and purified as described previously by Yodmuang *et al.* (61). *Artemia* adults (nauplius destined) were injected with 1 μg of *Ar*-CFTR dsRNA or GFP dsRNA by using an Ultra-MicroPump II instrument equipped with a Micro4TM MicroSyringe pump controller (World Precision Instruments). After injection, the animals were cultured in 40‰ artificial seawater. One week later the samples were collected.

CFTR siRNA (sense, GCUGUGUCUGUAAACUGAUGGCUAA; and antisense, UUAGCCAUCAGUUUACAGACACAGC) were designed, and SKOV3 and HT-29 cells were transfected with CFTR siRNA and the scramble. Cell transfections were performed with Lipofectamine 3000 (Invitrogen) as recommended by the manufacturer.

Immunofluorescence

Artemia samples were fixed with 4% paraformaldehyde and embedded with paraffin. Tissue slides (5 μm thick) were treated with 0.25% Triton X-100 for 10 min. The slides were blocked in antiserum dilution buffer containing 1% BSA and 0.1% Triton X-100 for 1 h and then incubated with appropriate antibodies at 4 °C overnight. The slides were incubated in a secondary FITC-conjugated 594 antibody (Invitrogen) for 2 h, and the nuclei were counterstained with 4′,6-diamidino-2-phenylindole (DAPI) (Sangon Biotech, Shanghai, China). All confocal images were collected by using a Zeiss LSM 710 (Carl Zeiss) confocal microscope equipped with a 40×, 1.4-numerical aperture objective lens.

EdU-labeled assay

MCF-7 cells were treated with 10 μM GlyH-101 (MedChem Express, Monmouth Junction, NJ) for 24 h, and then immunofluorescence was performed as previously described using Ki67 antibodies (Abcam) with a secondary FITC-conjugated 594 antibody. DNA synthesis activity in GlyH-101–treated cells was studied using the EdU-DNA synthesis assay. Cell-Light™ EdU Apollo® 643 *in vitro* imaging kit (RiboBio, Guangzhou, China) was used according to the supplier's protocol. EdU was added to the culture media at 50 μM, and after 2 h, the cells were fixed in 4% paraformaldehyde for 30 min, permeated with 0.25% Trixon X-100 for 10 min, and stained with 10 μM Apollo 643 for 30 min. The nuclei were counterstained with DAPI, and the cells were analyzed by confocal laser-scanning microscope.

Membrane potential measurements

For live cell staining, the cysts were crushed in 1× PBS using Disposable PELLET PESTLES (Kimble Chase Life Science and Research Products) gently by hand and blown a few times to spread the cells apart. After 2–3 min standing, the upper phase was centrifuged at 1500 rpm for 5 min, and the precipitation was washed twice with 1× PBS. V_{mem} was measured using the membrane potential–sensitive dye $DiBAC_4(3)$ (Invitrogen). Upon transmembrane depolarization, the $DiBAC_4(3)$ enters the cell and binds to protein molecules, acquiring enhanced fluorescence. By contrast, fluorescence intensity is reduced when the membrane is hyperpolarized. After incubation with 0.5 μM $DiBAC_4(3)$ for 30 min at 37 °C, the cells were analyzed by Zeiss 510 (Carl Zeiss) confocal laser-scanning microscope with excitation at 488 nm and emission measured at 518 nm.

Chloride concentration measurements

Live cells were incubated with 8 mM MQAE (Invitrogen) for 1 h at 37 °C and rinsed with Ringer's standard solution. The MQAE fluorescence was analyzed by Zeiss 510 confocal laser-scanning microscope with excitation at 353 nm and emission measured at 460 nm.

Potassium and sodium concentration measurements

Live cells were incubated with 10 μM ANG-2/AM (Asante Potassium Green-2 AM; Abcam) or 10 μM CoroNa (CoroNa™ Green; Invitrogen) for 30 min at 37 °C under a dark condition, followed by washing twice with 1× PBS, and the cells were analyzed by Zeiss 510 confocal laser-scanning microscope with excitation at 488 nm and emission measured at 540 nm.

Cell culture

MCF-7 cells were cultured in eagle's minimum essential medium (EMEM) (Genom, Hangzhou, China), SKOV3 cells were cultured in Dulbecco's modified Eagle's medium (Genom), and HT-29 cells were cultured in 1640 (Genom) at 37 °C in 5% CO_2, supplemented with 10% fetal bovine serum (Gibco), 100 IU/ml penicillin, and 100 μg/ml streptomycin (Sigma–Aldrich).

Cell-cycle analysis

Fixed cells were treated with 100 μg/ml RNase A (Sigma) and stained for 30 min with 50 μg/ml propidium iodide (Sigma) at 4 °C. Cell cycle analysis was performed on a Beckman Coulter flow cytometer (FC-500MCL). The analysis of quantification depending on the raw data was manually adjusted by the FITTING parameter.

Patch-clamp recording

Data acquisition and recording methods were as those reported previously (62). Whole-cell patch-clamp recordings were performed on the AXON 700B. Cells were superfused with solution containing 160 mM NaCl, 2.5 mM KCl, 5 mM $CaCl_2$, 1 mM $MgCl_2$, 10 mM HEPES, 8 mM D-glucose, pH 7.4, with NaOH.

Cell proliferation assay

Cell proliferation was assessed using CCK-8 kit (Beyotime Biotechnology, Shanghai, China). The cells were planted in

96-well plates (1000 cells/well) in triplicate. After 24 h, the cells were treated with GlyH-101 or transfected with siRNA for days and used the Multiskan EX plate reader (Thermo Fisher Scientific) to quantify the viable cells by measuring absorbance at 450 nM.

RNA-Seq analysis

The mRNA-Seq experiments were performed by Novogene (Beijing, China). mRNA-Seq library was prepared for sequencing using standard Illumina protocols. Briefly, total RNA from MCF-7 with or without GlyH-101 treatment was isolated using TRIzol reagent and treated with RNase-free DNase I (New England Biolabs) to remove any contaminating genomic DNA. mRNA extraction was performed using Dynabeads oligo(dT) (Invitrogen). Double-stranded complementary DNAs were synthesized using Superscript II reverse transcriptase (Invitrogen) and random hexamer primers. The cDNAs were then fragmented by nebulization, and the standard Illumina protocol was followed thereafter to create the mRNA-Seq library. For the data analysis, base calls were performed using CASAVA. Reads were aligned to the genome using the split read aligner TopHat (v2.0.7) and Bowtie2, using default parameters. HTSeq was used for estimating their abundances. Differential expression analysis of two conditions/groups (two biological replicates per condition) was performed using the DESeq R package (1.18.0). GO enrichment analysis of differentially expressed genes was implemented by the GOseq R package, in which gene length bias was corrected. GO terms with corrected p value less than 0.05 were considered significantly enriched by differential expressed genes.

The *Artemia* mRNA-Seq experiments were performed by Sangon (Shanghai, China). Total RNA from nauplius-destined ovoviviparous embryos, prediapause embryos, diapause embryos, and postdiapause embryos was extracted as above described. RNA integrity was evaluated with a 1.0% agarose gel. Thereafter, the quality and quantity of RNA were assessed using a Nano Photometer® spectrophotometer (IMPLEN) and an Agilent 2100 Bioanalyzer (Agilent Technologies). Sequencing libraries were generated using VAHTSTM mRNA-Seq V2 Library prep kit for Illumina® following the manufacturer's recommendations, and index codes were added to attribute sequences to each sample. Paired-end sequencing of the library was performed on the HiSeq XTen sequencers (Illumina, San Diego, CA). FastQC (version 0.11.2) was used for evaluating the quality of sequenced data. Unigenes were blasted against NCBI Nr (NCBI nonredundant protein database), SwissProt, TrEMBL, Conserved Domain Database, Pfam, and KOG (Eukaryotic Orthologous Groups) databases (E-value $<$ 1e-5). At the same time, TransDecoder (version 3.0.1) was used to predict CDS sequences of the unaligned Unigenes.

Statistics and quantification

The sample size for each experiment is indicated in the figure legend. The data are presented as the means ± S.D. For two groups of data, a two-tail Student's t test was used. For three or more groups, the data were analyzed using a one-way analysis of variance. p values less than 0.05 were considered significant, and p values less than 0.01 were considered to be highly significant. For information on quantification of fluorescence ($DiBAC_4(3)$/MQAE), we used 15 cells for immunofluorescent observation. All data represent the averages of at least three independent experiments.

Author contributions—A.-Q. L., J.-S. Y., and W.-J. Y. data curation; A.-Q. L., Z.-P. S., and F. J. formal analysis; A.-Q. L. and W.-J. Y. visualization; A.-Q. L., Z.-P. S., X. L., F. J., L. Z., and W.-H. J. methodology; A.-Q. L. and W.-J. Y. writing-original draft; Z.-P. S. and J.-S. Y. software; Z.-P. S., X. L., F. J., and W.-J. Y. investigation; J.-S. Y. and W.-J. Y. funding acquisition; J.-S. Y., S. D. V., G. V. S., P. B., and W.-J. Y. writing-review and editing; S. D. V., G. V. S., and P. B. resources; W.-J. Y. conceptualization; W.-J. Y. supervision; W.-J. Y. validation; W.-J. Y. project administration; S. D. V., G. V. S., and P. B. analyzed the Ar-CFTR sequence of parthenogenetic Artemia.

Acknowledgments—We express our sincere gratitude to Chris Wood for critical reading of the manuscript. We are also grateful to She-Long Zhang (College of Life Sciences, Zhejiang University, Hangzhou, China) for technical assistance with the confocal microscope and Chao Sun (Center of Analysis and Measurement, Zhejiang University, Hangzhou, China) for technical assistance with flow cytometry.

References

1. Coller, H. A., Sang, L., and Roberts, J. M. (2006) A new description of cellular quiescence. *PLoS Biol.* **4,** e83 CrossRef Medline
2. Yao, G. (2014) Modelling mammalian cellular quiescence. *Interface Focus* **4,** 20130074 CrossRef Medline
3. Gray, J. V., Petsko, G. A., Johnston, G. C., Ringe, D., Singer, R. A., and Werner-Washburne, M. (2004) "Sleeping beauty": quiescence in *Saccharomyces cerevisiae*. *Microbiol. Mol. Biol. Rev.* **68,** 187–206 CrossRef Medline
4. Cheung, T. H., and Rando, T. A. (2013) Molecular regulation of stem cell quiescence. *Nat. Rev. Mol. Cell Biol.* **14,** 329–340 CrossRef Medline
5. Nakamura-Ishizu, A., Takizawa, H., and Suda, T. (2014) The analysis, roles and regulation of quiescence in hematopoietic stem cells. *Development* **141,** 4656–4666 CrossRef Medline
6. Stuart, J. A., and Brown, M. F. (2006) Energy, quiescence and the cellular basis of animal life spans. *Comp. Biochem. Physiol. A Mol. Integr. Physiol.* **143,** 12–23 CrossRef Medline
7. Lirakis, M., Dolezal, M., and Schlötterer, C. (2018) Redefining reproductive dormancy in *Drosophila* as a general stress response to cold temperatures. *J. Insect Physiol.* **107,** 175–185 CrossRef Medline
8. Lubzens, E., Cerda, J., and Clark, M. (2010) *Dormancy and Resistance in Harsh Environments*, Springer, New York
9. Valcourt, J. R., Lemons, J. M., Haley, E. M., Kojima, M., Demuren, O. O., and Coller, H. A. (2012) Staying alive: metabolic adaptations to quiescence. *Cell Cycle* **11,** 1680–1696 CrossRef Medline
10. Sundelacruz, S., Levin, M., and Kaplan, D. L. (2009) Role of membrane potential in the regulation of cell proliferation and differentiation. *Stem Cell Reviews* **5,** 231–246 CrossRef Medline
11. Wright, S. H. (2004) Generation of resting membrane potential. *Adv. Physiol. Educ.* **28,** 139–142 CrossRef Medline
12. Yang, M., and Brackenbury, W. J. (2013) Membrane potential and cancer progression. *Front. Physiol.* **4,** 185 Medline
13. Ransom, C. B., and Sontheimer, H. (1995) Biophysical and pharmacological characterization of inwardly rectifying K^+ currents in rat spinal cord astrocytes. *J. Neurophysiol.* **73,** 333–346 CrossRef Medline
14. Bordey, A., and Sontheimer, H. (1997) Postnatal development of ionic currents in rat hippocampal astrocytes in situ. *J. Neurophysiol.* **78,** 461–477 CrossRef Medline
15. Brodwick, M. S. (1983) Ion channels: membrane potential-dependent ion channels in cell membrane. *Science* **222,** 1115–1116 CrossRef Medline
16. Inagaki, C., Hara, M., and Inoue, M. (1992) [Neuronal intracellular chloride ion concentrations and their regulatory mechanisms]. *Folia Pharmacologica Japonica* **99,** 307–315 CrossRef Medline

17. Novak, I., Pedersen, P. S., and Larsen, E. H. (1992) Chloride and potassium conductances of cultured human sweat ducts. *Pfluegers Arch.* **422,** 151–158 CrossRef Medline
18. Hyde, S. C., Emsley, P., Hartshorn, M. J., Mimmack, M. M., Gileadi, U., Pearce, S. R., Gallagher, M. P., Gill, D. R., Hubbard, R. E., and Higgins, C. F. (1990) Structural model of ATP-binding proteins associated with cystic fibrosis, multidrug resistance and bacterial transport. *Nature* **346,** 362–365 CrossRef Medline
19. Sheppard, D. N., and Welsh, M. J. (1999) Structure and function of the CFTR chloride channel. *Physiol. Rev.* **79,** S23–S45 CrossRef Medline
20. Schwiebert, E. M., Egan, M. E., Hwang, T. H., Fulmer, S. B., Allen, S. S., Cutting, G. R., and Guggino, W. B. (1995) CFTR regulates outwardly rectifying chloride channels through an autocrine mechanism involving ATP. *Cell* **81,** 1063–1073 CrossRef Medline
21. Lee, M. G., Wigley, W. C., Zeng, W., Noel, L. E., Marino, C. R., Thomas, P. J., and Muallem, S. (1999) Regulation of Cl^-/HCO_3^- exchange by cystic fibrosis transmembrane conductance regulator expressed in NIH 3T3 and HEK 293 cells. *J. Biol. Chem.* **274,** 3414–3421 CrossRef Medline
22. Wei, L., Vankeerberghen, A., Cuppens, H., Eggermont, J., Cassiman, J. J., Droogmans, G., and Nilius, B. (1999) Interaction between calcium-activated chloride channels and the cystic fibrosis transmembrane conductance regulator. *Pfluegers Arch.* **438,** 635–641 Medline
23. Reddy, M. M., and Quinton, P. M. (2005) ENaC activity requires CFTR channel function independently of phosphorylation in sweat duct. *J. Membr. Biol.* **207,** 23–33 CrossRef Medline
24. Scriver, C. R. (1995) *The Metabolic and Molecular Bases of Inherited Disease*, 7th Ed., McGraw-Hill, Health Professions Division, New York
25. Montoro, D. T., Haber, A. L., Biton, M., Vinarsky, V., Lin, B., Birket, S. E., Yuan, F., Chen, S., Leung, H. M., Villoria, J., Rogel, N., Burgin, G., Tsankov, A. M., Waghray, A., Slyper, M., Waldman, J., *et al.* (2018) A revised airway epithelial hierarchy includes CFTR-expressing ionocytes. *Nature* **560,** 319–324 CrossRef Medline
26. Plasschaert, L. W., Zilionis, R., Choo-Wing, R., Savova, V., Knehr, J., Roma, G., Klein, A. M., and Jaffe, A. B. (2018) A single-cell atlas of the airway epithelium reveals the CFTR-rich pulmonary ionocyte. *Nature* **560,** 377–381 CrossRef Medline
27. Browne, R. A., Sorgeloos, P., and Trotman, C. N. A. (1991) *Artemia Biology*, pp. 37–73, CRC Press, Boca Raton, FL
28. Abatzopoulos, T. J. (2002) *Artemia: Basic and Applied Biology*, pp. 129–170, Kluwer Academic, London
29. Dai, J. Q., Zhu, X. J., Liu, F. Q., Xiang, J. H., Nagasawa, H., and Yang, W. J. (2008) Involvement of p90 ribosomal S6 kinase in termination of cell cycle arrest during development of Artemia-encysted embryos. *J. Biol. Chem.* **283,** 1705–1712 CrossRef Medline
30. Li, R., Chen, D. F., Zhou, R., Jia, S. N., Yang, J. S., Clegg, J. S., and Yang, W. J. (2012) Involvement of Polo-like kinase 1 (Plk1) in mitotic arrest by inhibition of mitogen-activated protein kinase-extracellular signal-regulated kinase-ribosomal S6 kinase 1 (MEK–ERK–RSK1) cascade. *J. Biol. Chem.* **287,** 15923–15934 CrossRef Medline
31. Yang, F., Jia, S. N., Yu, Y. Q., Ye, X., Liu, J., Qian, Y. Q., and Yang, W. J. (2012) Deubiquitinating enzyme BAP1 is involved in the formation and maintenance of the diapause embryos of Artemia. *Cell Stress Chaperones* **17,** 577–587 CrossRef Medline
32. Zhou, R., Yang, F., Chen, D. F., Sun, Y. X., Yang, J. S., and Yang, W. J. (2013) Acetylation of chromatin-associated histone H3 lysine 56 inhibits the development of encysted Artemia embryos. *PLoS One* **8,** e68374 CrossRef Medline
33. Chen, D. F., Lin, C., Wang, H. L., Zhang, L., Dai, L., Jia, S. N., Zhou, R., Li, R., Yang, J. S., Yang, F., Clegg, J. S., Nagasawa, H., and Yang, W. J. (2016) An La-related protein controls cell cycle arrest by nuclear retrograde transport of tRNAs during diapause formation in Artemia. *BMC Biol.* **14,** 16 CrossRef Medline
34. Dai, L., Ye, S., Li, H. W., Chen, D. F., Wang, H. L., Jia, S. N., Lin, C., Yang, J. S., Yang, F., Nagasawa, H., and Yang, W. J. (2017) SETD4 regulates cell quiescence and catalyzes the trimethylation of H4K20 during diapause formation in Artemia. *Mol. Cell. Biol.* **37,** e00453-16 Medline
35. Clegg, J. S., Jackson, S. A., Liang, P., and MacRae, T. H. (1995) Nuclear-cytoplasmic translocations of protein p26 during aerobic-anoxic transitions in embryos of *Artemia franciscana*. *Exp. Cell Res.* **219,** 1–7 CrossRef Medline
36. Liang, P., and MacRae, T. H. (1999) The synthesis of a small heat shock/α-crystallin protein in Artemia and its relationship to stress tolerance during development. *Dev. Biol.* **207,** 445–456 CrossRef Medline
37. Binggeli, R., and Weinstein, R. C. (1986) Membrane potentials and sodium channels: hypotheses for growth regulation and cancer formation based on changes in sodium channels and gap junctions. *J. Theor. Biol.* **123,** 377–401 CrossRef Medline
38. Yasuda, T., Bartlett, P. F., and Adams, D. J. (2008) K(ir) and K(v) channels regulate electrical properties and proliferation of adult neural precursor cells. *Mol. Cell. Neurosci.* **37,** 284–297 CrossRef Medline
39. Kunzelmann, K. (2005) Ion channels and cancer. *J. Membr. Biol.* **205,** 159–173 CrossRef Medline
40. Liang, W., Ray, J. B., He, J. Z., Backx, P. H., and Ward, M. E. (2009) Regulation of proliferation and membrane potential by chloride currents in rat pulmonary artery smooth muscle cells. *Hypertension* **54,** 286–293 CrossRef Medline
41. Tang, Y. B., Liu, Y. J., Zhou, J. G., Wang, G. L., Qiu, Q. Y., and Guan, Y. Y. (2008) Silence of ClC-3 chloride channel inhibits cell proliferation and the cell cycle via G/S phase arrest in rat basilar arterial smooth muscle cells. *Cell Proliferation* **41,** 775–785 CrossRef Medline
42. Zheng, Y. J., Furukawa, T., Tajimi, K., and Inagaki, N. (2003) Cl^- channel blockers inhibit transition of quiescent (G_0) fibroblasts into the cell cycle. *J. Cell. Physiol.* **194,** 376–383 CrossRef Medline
43. Blackiston, D. J., McLaughlin, K. A., and Levin, M. (2009) Bioelectric controls of cell proliferation: ion channels, membrane voltage and the cell cycle. *Cell Cycle* **8,** 3527–3536 CrossRef Medline
44. Kito, H., Yamamura, H., Suzuki, Y., Ohya, S., Asai, K., and Imaizumi, Y. (2014) Membrane hyperpolarization induced by endoplasmic reticulum stress facilitates Ca^{2+} influx to regulate cell cycle progression in brain capillary endothelial cells. *J. Pharmacol. Sci.* **125,** 227–232 CrossRef Medline
45. Wang, W., Fan, Y., Wang, S., Wang, L., He, W., Zhang, Q., and Li, X. (2014) Effects of voltage-gated K^+ channel on cell proliferation in multiple myeloma. *ScientificWorldJournal* **2014,** 785140 Medline
46. Petrik, D., Myoga, M. H., Grade, S., Gerkau, N. J., Pusch, M., Rose, C. R., Grothe, B., and Götz, M. (2018) Epithelial sodium channel regulates adult neural stem cell proliferation in a flow-dependent manner. *Cell Stem Cell* **22,** 865–878.e8 CrossRef Medline
47. Woodfork, K. A., Wonderlin, W. F., Peterson, V. A., and Strobl, J. S. (1995) Inhibition of ATP-sensitive potassium channels causes reversible cell-cycle arrest of human breast cancer cells in tissue culture. *J. Cell. Physiol.* **162,** 163–171 CrossRef Medline
48. Chittajallu, R., Chen, Y., Wang, H., Yuan, X., Ghiani, C. A., Heckman, T., McBain, C. J., and Gallo, V. (2002) Regulation of Kv1 subunit expression in oligodendrocyte progenitor cells and their role in G_1/S phase progression of the cell cycle. *Proc. Natl. Acad. Sci. U.S.A.* **99,** 2350–2355 CrossRef Medline
49. Barman, P. P., Choisy, S. C., Gadeberg, H. C., Hancox, J. C., and James, A. F. (2011) Cardiac ion channel current modulation by the CFTR inhibitor GlyH-101. *Biochem. Biophys. Res. Commun.* **408,** 12–17 CrossRef Medline
50. König, J., Schreiber, R., Voelcker, T., Mall, M., and Kunzelmann, K. (2001) The cystic fibrosis transmembrane conductance regulator (CFTR) inhibits ENaC through an increase in the intracellular Cl^- concentration. *EMBO Reports* **2,** 1047–1051 CrossRef Medline
51. Fleming, H. E., Janzen, V., Lo Celso, C., Guo, J., Leahy, K. M., Kronenberg, H. M., and Scadden, D. T. (2008) Wnt signaling in the niche enforces hematopoietic stem cell quiescence and is necessary to preserve self-renewal *in vivo*. *Cell stem cell* **2,** 274–283 CrossRef Medline
52. Froeling, F. E., Feig, C., Chelala, C., Dobson, R., Mein, C. E., Tuveson, D. A., Clevers, H., Hart, I. R., and Kocher, H. M. (2011) Retinoic acid-induced pancreatic stellate cell quiescence reduces paracrine Wnt–β-catenin signaling to slow tumor progression. *Gastroenterology* **141,** 1486–1497.e1–14 CrossRef Medline
53. Liu, Y., Elf, S. E., Miyata, Y., Sashida, G., Liu, Y., Huang, G., Di Giandomenico, S., Lee, J. M., Deblasio, A., Menendez, S., Antipin, J., Reva, B., Koff, A., and Nimer, S. D. (2009) p53 regulates hematopoietic stem cell quiescence. *Cell Stem Cell* **4,** 37–48 CrossRef Medline

54. Kongsuphol, P., Cassidy, D., Hieke, B., Treharne, K. J., Schreiber, R., Mehta, A., and Kunzelmann, K. (2009) Mechanistic insight into control of CFTR by AMPK. *J. Biol. Chem.* **284,** 5645–5653 CrossRef Medline
55. Zhu, L., Yu, X. J., Xing, S., Jin, F., and Yang, W. J. (2018) Involvement of AMP-activated protein kinase (AMPK) in regulation of cell membrane potential in a gastric cancer cell line. *Sci. Rep.* **8,** 6028 CrossRef Medline
56. Brown, J. A., Yonekubo, Y., Hanson, N., Sastre-Perona, A., Basin, A., Rytlewski, J. A., Dolgalev, I., Meehan, S., Tsirigos, A., Beronja, S., and Schober, M. (2017) TGF-β–induced quiescence mediates chemoresistance of tumor-propagating cells in squamous cell carcinoma. *Cell Stem Cell* **21,** 650–664.e8 CrossRef Medline
57. Goddard, E. T., Bozic, I., Riddell, S. R., and Ghajar, C. M. (2018) Dormant tumour cells, their niches and the influence of immunity. *Nat. Cell Biol.* **20,** 1240–1249 CrossRef Medline
58. Saitou, N., and Nei, M. (1987) The neighbor-joining method: a new method for reconstructing phylogenetic trees. *Mol. Biol. Evol.* **4,** 406–425 Medline
59. Felsenstein, J. (1985) Confidence limits on phylogenies: an approach using the bootstrap. *Evolution* **39,** 783–791 CrossRef Medline
60. Kumar, S., Stecher, G., and Tamura, K. (2016) MEGA7: Molecular Evolutionary Genetics Analysis version 7.0 for bigger datasets. *Mol. Biol. Evol.* **33,** 1870–1874 CrossRef Medline
61. Yodmuang, S., Tirasophon, W., Roshorm, Y., Chinnirunvong, W., and Panyim, S. (2006) YHV-protease dsRNA inhibits YHV replication in *Penaeus monodon* and prevents mortality. *Biochem. Biophys. Res. Commun.* **341,** 351–356 CrossRef Medline
62. Baylie, R. L., Cheng, H., Langton, P. D., and James, A. F. (2010) Inhibition of the cardiac L-type calcium channel current by the TRPM8 agonist, (−)-menthol. *J. Physiol. Pharmacol.* **61,** 543–550 Medline

The chloride channel cystic fibrosis transmembrane conductance regulator (CFTR) controls cellular quiescence by hyperpolarizing the cell membrane during diapause in the crustacean *Artemia*

An-Qi Li, Zhan-Peng Sun, Xu Liu, Jin-Shu Yang, Feng Jin, Lin Zhu, Wen-Huan Jia, Stephanie De Vos, Gilbert Van Stappen, Peter Bossier and Wei-Jun Yang

J. Biol. Chem. 2019, 294:6598-6611.
doi: 10.1074/jbc.RA118.005900 originally published online February 14, 2019